

Accretion discs onto supermassive compact objects: a portal to dark matter physics in active galaxies

C. Millauro¹, C. R. Argüelles^{*2,3}, F. L. Vieyro^{4,5}, V. Crespi⁵, and M. F. Mestre^{3,5}

¹ Departamento de Física, Facultad de Ciencias Exactas y Naturales, Universidad de Buenos Aires, Pabellón I, Ciudad Universitaria, 1428 Buenos Aires, Argentina

² ICRA Net, Piazza della Repubblica 10, 65122 Pescara, Italy

³ Instituto de Astrofísica de La Plata, UNLP & CONICET, Paseo del Bosque, B1900FWA La Plata, Argentina

⁴ Instituto Argentino de Radioastronomía (IAR, CONICET/CIC/UNLP), C.C.5, (1894) Villa Elisa, Buenos Aires, Argentina

⁵ Fac. de Ciencias Astron. y Geofísicas, Universidad Nacional de La Plata, Paseo del Bosque, B1900FWA La Plata, Argentina

Received XX, XX; accepted XX, XX

ABSTRACT

Context. The study of the physics of accretion discs developed around the supermassive black hole (BH) candidates are essential theoretical tools to test their nature.

Aims. Here, we study the accretion flow and associated emission using generalised α -discs on to horizonless dark compact objects, in order to compare with the traditional BH scenario. The BH alternative here proposed consists in a dense and highly degenerate core made of fermionic dark matter (DM) which is surrounded by a more diluted DM halo. Such a *dense core–diluted halo* DM configuration is a solution of the Einstein equations of General Relativity (GR) in spherical symmetry, which naturally arises once the quantum nature of the DM fermions is fully accounted for.

Methods. The methodology followed in this work consist in first generalising the theory of α -discs to work in the presence of regular and horizonless compact objects, and second, to apply it to the case of *core-halo* DM profiles typical of active-like galaxies.

Results. The fact that the compactness of the dense and transparent DM core scales with the particle mass, allows for the following key findings of this work: (i) it always exist a given core compacity -i.e. corresponding particle mass- which produces a luminosity spectrum which is basically indistinguishable from that of a Schwarzschild BH of the same mass as the DM core; (ii) the disc can enter deep inside the non-rotating DM core, allowing for accretion powered efficiencies as high as 28%, thus comparable to that of a highly rotating Kerr BH.

Conclusions. These results, together with the existence of a critical DM core mass of collapse into a supermassive BH, open new avenues of research for two seemingly unrelated topics such as AGN phenomenology and dark matter physics.

Key words. Dark matter – Cosmology – Accretion, accretion disks

1. Introduction

One of the central results of the standard cosmological model *Lambda cold dark matter* (Λ CDM), is the necessity of invoking a dark matter component as an essential part in the composition of the Universe (Bahcall et al. 1999). However, how such a dark component of matter is distributed on inner galactic scales, and what is the nature and mass of the dark matter particles, still remain unclear (Bullock & Boylan-Kolchin 2017). A main available tool to tackle these questions is based on cosmological N-body (classical) simulations with adequate initial conditions, as for example the ones provided by the Λ CDM paradigm (see e.g. Ivanov et al. 2020 and references therein). Although this paradigm manages to explain in a good way the distribution of dark matter on large scales ($> \text{Mpc}$), it faces various challenges on short galactic scales (Diemand et al. 2005; Battaglia et al. 2008; Joung et al. 2009; Bullock & Boylan-Kolchin 2017).

Within the framework of cosmological simulations, different state-of-the-art alternatives are being provided to try to solve

these problems, including the possibility that cold DM is self-interacting (Kaplinghat et al. 2020), considering warm instead of cold DM (Bozek et al. 2019), or even abandoning the hypothesis of classical particles by incorporating quantum effects into the simulations (Schive et al. 2014). Along the line of including the quantum nature of the DM particles explicitly in the physics of the DM halos, it has been recently proposed an alternative (semi-analytical) approach for fermionic DM in a cosmological framework (Argüelles et al. 2021). It covers the problems of DM halo formation, overall morphology and stability, from first principle physics. In particular, it includes for (quantum) statistical mechanics and thermodynamics in the presence of self-gravity, offering solutions to some of the problems that the Λ CDM paradigm possesses at short scales (see e.g., Krut et al. 2023; Argüelles et al. 2023a for a recent work and a review, respectively).

Fermionic mass distributions of this sort are obtained by solving the equations of a self-gravitating system of neutral fermionic (spin 1/2) particles in hydrostatic and thermodynamic equilibrium in GR. Some generic solutions to this model were

* E-mail: carguelles@fcaglp.unlp.edu.ar

obtained in the past in different works aimed to the problem of DM halos (Chau et al. 1984; Ingrosso & Ruffini 1988; Gao et al. 1990; Chavanis & Sommeria 1998; Bilic et al. 2002; Chavanis 2006; Destri et al. 2013; Argüelles & Ruffini 2014; Ruffini et al. 2015; Chavanis et al. 2015), though only recently a more realistic version of this theory including for particle evaporation and central (fermion) degeneracy, was developed in GR in Argüelles et al. (2018, 2019, 2021) and is referred to as the (extended) Ruffini-Argüelles-Rueda (RAR) model¹. The model implies novel DM density profiles which self-consistently accounts for the Pauli exclusion principle, thus yielding a source of quantum pressure towards the centre of the configurations with key implications for galactic nuclei. The more general DM profiles develop a *dense core - diluted halo* morphology which, unlike other phenomenological profiles in the literature, depends on the mass of the particle. Remarkably, these fermionic DM halos can explain the galaxy rotation curves in different galaxy types (Argüelles et al. 2018, 2019; Krut et al. 2023), while the degenerate fermion core can mimic their central BHs (Argüelles et al. 2018, 2019; Becerra-Vergara et al. 2020; Argüelles et al. 2021; Becerra-Vergara et al. 2021; Argüelles et al. 2022b,a). Moreover, as demonstrated in Argüelles et al. (2021, 2023b); Argüelles et al. (2023) from dynamical and thermodynamical stability criteria in GR, the central DM core can reach a critical mass for collapse and thus providing a novel channel for supermassive BH formation in the early Universe (see also Chavanis & Alberti 2019; Alberti & Chavanis 2020 for a first dynamical and thermodynamical instability study in GR of the self-gravitating Fermi gas at finite temperature leading to a BH formation).

In this work we will centre our attention on fermionic *core-halo* profiles applied to typical active-like galaxies, together with their central accretion processes. The study of the free parameters of the theory (including particle mass) will be focused in solutions whose central core has not yet reached the critical mass for collapse, and thus it will represent an alternative to the traditional BH scenario. This choice is being motivated by the ambitious endeavour of trying to understand the very nature of the massive compact objects at galaxy centres, their formation channel, surrounding emission, and finally their relation with the host galaxy and AGN phenomenology.

Motivated by distinct branches of theoretical physics and astrophysics, different alternative models to that of the classical BHs have been proposed to date (see e.g. Cardoso & Pani 2019 for a review). When dealing with galaxy centres, a typical example studied in the recent past are boson stars (Schunck & Mielke 1999; Torres et al. 2000; Guzmán 2006; Vincent et al. 2016; Olivares et al. 2020), that is, horizonless and massive compact objects made of self-gravitating scalar fields. In particular, different observational signatures of boson stars were studied, such as the luminosity spectra of α -discs (Guzmán 2006); strong-field images and luminosity patterns in boson stars surrounded by a disc torus (Vincent et al. 2016); and a detailed study of the accretion flow via general relativistic magnetohydrodynamic simulations in the space-time of a boson star (Olivares et al. 2020).

In analogy to the above cases of study, it is our objective to start a research program for AGN phenomenology dedicated to the RAR model for a self-gravitating system of fermions as DM in galaxies. Thus, in order to cover the main observational signatures associated to the emission of galaxy centres, we start in this work by studying the accretion and corresponding luminosity of barionic matter onto supermassive compact cores made of

fermionic DM. This will be done by first extending the standard disc model of Shakura & Sunyaev (Shakura & Sunyaev 1973) in presence of a fermionic DM distribution, using a Keplerian disc and a classical treatment. In the case of fermionic particles, the main motivation comes via the numerous efforts made in the last decade to shed light on the nature of such supermassive dark compact objects and the surrounding DM halo in a unified description (Argüelles et al. 2023a).

With the data coming from the observational campaigns dedicated to the stellar motions around Sgr A* (Ghez et al. 2005, 2008; Genzel et al. 2010; Gravity Collaboration et al. 2018) - confirming the presence of a supermassive compact object- it has been shown that the core-halo RAR solutions accurately reproduce the orbital motion of the S stars including its relativistic effects (Becerra-Vergara et al. 2020, 2021; Argüelles et al. 2022c). Additionally, the observations of the relativistic images using Very Long Base Interferometry (VLBI) in both M87 and the Milky Way (Collaboration et al. 2019; Akiyama et al. 2022), motivate to further test the RAR solution for which it is essential to study the accretion physics in this new paradigm.

The article is organised as follows: we briefly describe the extended RAR model in Sec. 2. In Sec. 3, we study the efficiency, spectra as well as solutions of steady-state thin discs which accrete in the background metric of the RAR model, and in Sec. 4 we present the conclusions of the work.

2. Extended RAR model

2.1. The model

The RAR model consists on a spherical system of self-gravitating tempered fermions which are distributed in phase-space according to the following Fermi-Dirac-like distribution function:

$$f_c(\epsilon \leq \epsilon_c) = \frac{2}{h^3} \frac{1 - e^{(\epsilon - \epsilon_c)/kT}}{e^{(\epsilon - \mu)/kT} + 1}, \quad f_c(\epsilon > \epsilon_c) = 0. \quad (1)$$

With $\epsilon = \sqrt{c^2 p^2 + m^2 c^4} - mc^2$ the particle kinetic energy, μ is the chemical potential with the particle rest-energy subtracted off, T is the effective temperature, k is the Boltzmann constant, h is the Planck constant, c is the speed of light, and m is the fermion mass. Anti-fermions are not included as temperatures $T \ll mc^2/k$ are considered. The full set of (functional) dimensionless-parameters of the model is defined by the temperature, degeneracy and cutoff parameters, $\beta = kT/(mc^2)$, $\theta = \mu/kT$, $W = \epsilon_c/(kT)$ respectively.

Interestingly, a coarse-grained phase-space distribution of this kind can be linked with halo formation processes, since it can be obtained from a generalised kinetic theory in presence of gravity as demonstrated in Chavanis (2004). Indeed, it was shown there that Eq. 1 is a (quasi-) stationary solution of a generalised Fokker-Planck equation for fermions (Chavanis 2004, 2006). Such a kinetic theory includes the physics of violent relaxation appropriate for nonlinear structure formation -as originally presented in Lynden-Bell (1967) for classical particles- though further extended including for particle evaporation and applied to realistic DM halos (Chavanis et al. 2015; Argüelles et al. 2021). This kind of phase-space distributions have been shown to fulfil a maximisation entropy principle during the collisionless relaxation process, until the halo reaches the steady state which is currently observed. More recently, this formation mechanism of fermionic halos was applied in Krut et al. (2023) for a sample of 120 galaxies, and compared with phenomenological profiles as obtained from cosmological N-body simulations.

¹ The term ‘relativistic fermionic King model’ is also used in the literature (Chavanis 2022).

The corresponding 4-parametric fermionic equations of state, at given radius r , $\rho(\beta, \theta, W, m)$, $P(\beta, \theta, W, m)$, are directly obtained as the corresponding integrals (bounded from above by $\epsilon \leq \epsilon_c$) of $f_c(p)$. These components are the diagonal part of the stress–energy tensor in the Einstein equations, which are solved under the perfect fluid approximation within a background metric with spherical symmetry, which reads

$$ds^2 = e^\nu c^2 dt^2 - e^\lambda dr^2 - r^2 d\Theta^2 - r^2 \sin^2 \Theta d\phi^2, \quad (2)$$

with (r, Θ, ϕ) the spherical coordinates, and ν and λ only depending on the radial coordinate r . The system of Einstein equations (that is mass and TOV equations below) is solved together with the Tolman and Klein thermodynamic equilibrium conditions (involved in Eqs. 5–6 below), and (particle) energy conservation along a geodesic (Eq. 7 below). The dimensionless system of highly-nonlinear ordinary differential equations reads:

$$\frac{d\hat{M}_{DM}}{d\hat{r}} = 4\pi\hat{r}^2\hat{\rho}, \quad (3)$$

$$\frac{d\nu}{d\hat{r}} = \frac{2(\hat{M}_{DM} + 4\pi\hat{P}\hat{r}^3)}{\hat{r}^2(1 - 2\hat{M}_{DM}/\hat{r})}, \quad (4)$$

$$\frac{d\theta}{d\hat{r}} = -\frac{1 - \beta_0(\theta - \theta_0)}{\beta_0} \frac{\hat{M}_{DM} + 4\pi\hat{P}\hat{r}^3}{\hat{r}^2(1 - 2\hat{M}_{DM}/\hat{r})}, \quad (5)$$

$$\beta(\hat{r}) = \beta_0 e^{\frac{\nu_0 - \nu(\hat{r})}{2}}, \quad (6)$$

$$W(\hat{r}) = W_0 + \theta(\hat{r}) - \theta_0, \quad (7)$$

where the dimensionless quantities are: $\hat{r} = r/\chi$, $\hat{M}_{DM} = GM_{DM}/(c^2\chi)$, $\hat{\rho} = G\chi^2\rho/c^2$, $\hat{P} = G\chi^2P/c^4$, with $\chi = 2\pi^{3/2}(\hbar/(mc))(m_p/m)$ and $m_p = \sqrt{\hbar c/G}$ the Planck mass. The system of Eqs. 3–7 constitute a boundary condition problem which, for fixed DM particle mass m , has to be solved for given set of free parameters (β_0, θ_0, W_0) defined at the centre of the configuration.

The most general solution results in a degenerate compact core (governed by Pauli degeneracy pressure), surrounded by an extended and more diluted halo (governed by thermal pressure) as detailed in section below and in Argüelles et al. (2018). The core mass $M_c = M_{DM}(r_c)$ is given at the core radius, defined as the first maximum of the rotation curve. It corresponds with the radius where the central density has decreased about one tenth of the central value, i.e. where fermion degeneracy starts to vanish. In the following section we show different solutions for well motivated values of m , having DM core masses and total halo masses typical of active-like galaxies following Argüelles et al. (2019).

2.2. Application to active-like galaxies

The application of the extended RAR model to large galaxies with dark and regular compact cores reaching mass values of $\sim 10^7 - 10^8 M_\odot$ typical of AGN, was first shown in Argüelles et al. (2019). This was done for a DM particle mass $m \approx 50$ keV motivated by the excellent results obtained for the Milky Way (Argüelles et al. 2018; Becerra-Vergara et al. 2020, 2021; Argüelles et al. 2022c), where the corresponding

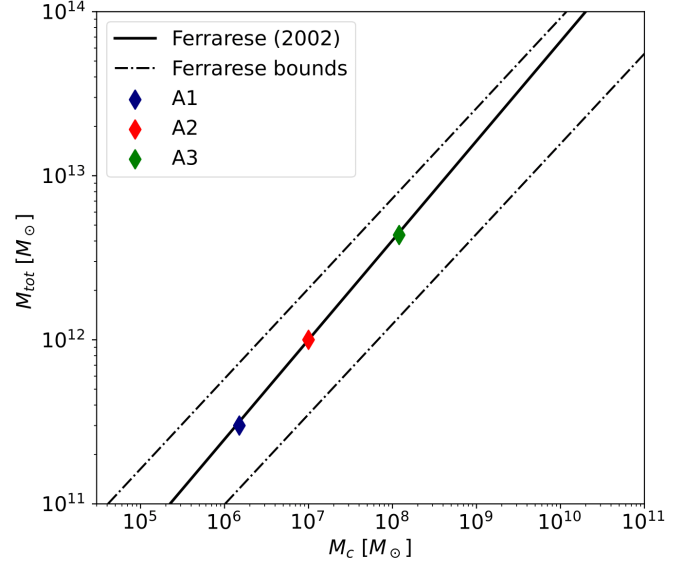


Fig. 1: *core-halo* RAR solutions for DM particle mass of $mc^2 = 48$ keV, in agreement with the Ferrarese relation connecting the halo mass with the supermassive central object mass (Ferrarese 2002).

DM core explains the motion of the S-cluster stars around Sgr A*. For such value of the fermion mass, the highly degenerate core reaches the critical mass of collapse M_c^{cr} into a SMBH of $\approx 2 \times 10^8 M_\odot$ (Argüelles et al. 2021). Particle masses of the order of $\sim 100 - 350$ keV have also been analysed within this DM model with excellent results (see Argüelles et al. 2018, 2023b). As demonstrated in Argüelles & Ruffini (2014); Argüelles et al. (2021) the larger the m the lower the critical core masses $M_c^{cr} \approx M_{OV} \propto 1/m^2$ (roughly following the Oppenheimer-Volkoff limit Oppenheimer & Volkoff 1939), with $m \approx 350$ keV leading to a critical mass of a DM core collapsing to a SMBH of $\approx 4 \times 10^6 M_\odot$ as for SgrA* (Argüelles et al. 2018; Becerra-Vergara et al. 2020).

An important prediction of the *core-halo* family of RAR DM profiles for given m , is that it can answer for different universal scaling relations such as: the Ferrarese relation (Ferrarese 2002; Bogdán & Goulding 2015) connecting the halo and its supermassive central object masses; the DM surface density relation (Donato et al. 2009), and the radial acceleration relation (McGaugh et al. 2016); as shown in (Argüelles et al. 2019; Krut et al. 2023). Indeed, in Fig. 1 we show an example of RAR profiles with $m = 48$ keV (solutions A1 – A3), corresponding to a halo mass window $M_{tot} \sim 10^{11} - 10^{12} M_\odot$ and supermassive DM compact objects of mass $M_c \sim 10^6 - 10^8 M_\odot$ in excellent agreement with the Ferrarese relation (RAR models with $m = 200$ keV are also in agreement with the correlation though reaching up to $M_c \sim 10^7 M_\odot$).

One of the central objectives of this work is to analyse the accretion power efficiencies, and consequent luminosity spectrum, caused by supermassive compact objects alternative to BHs. Due to the fact that larger fermion masses imply more compact and denser DM cores at given core mass (see e.g. Argüelles et al. (2018)), we will then study here two different families of profiles: the ones with $mc^2 = 48$ keV (which we call RAR model A), and the ones with $mc^2 = 200$ keV (referring to the RAR model B). In Table 1 we show the main parameters of both models: for a typical DM compact-core mass of $10^7 M_\odot$, the model B2 gives a more compact core with respect to the A2 solution

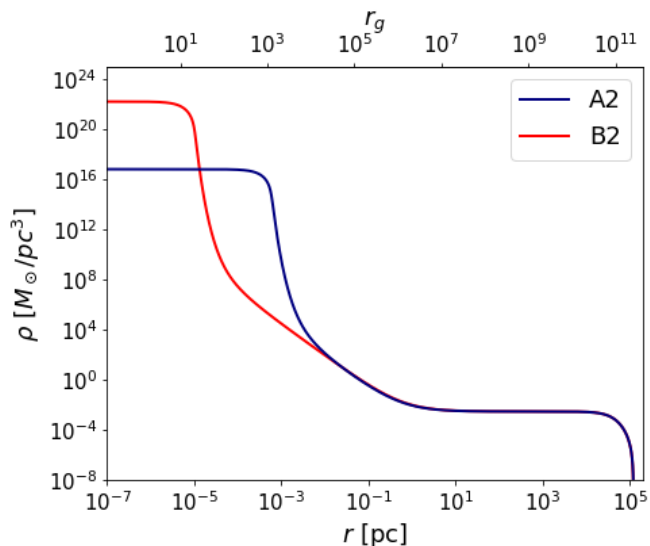


Fig. 2: Density profiles corresponding to core mass of $M_c = 1.0 \times 10^7 M_\odot$, and particle masses of $mc^2 = 48$ keV (A2, blue) and $mc^2 = 200$ keV (B2, red). These DM halos correspond to typical Elliptical galaxies.

(see Fig. 2 for a comparison between both profiles). The DM core mass in solution B2 is close to the critical mass of gravitational collapse to a Schwarzschild BH of that mass and thus implying very similar metric functions (see Fig. 3).

In Fig. 2 we show the density profiles for models A2 and B2. They clearly show the existence of compact and massive cores corresponding with the highest density trends, and the diluted halo at larger radii. This is because the system goes from being governed by fermionic degeneracy pressure at small radii, to be governed by thermal pressure at larger radii. Thus, the density profile transitions from a degenerate core of almost constant density to a Boltzmann-like regime in the outer halo, where the density falls off as a power-law followed by an exponential decrease determining the galaxy border.

3. Accretion discs

3.1. Efficiency

There is an essential difference between the Schwarzschild BH solution and the RAR DM model regarding the motion of massive particles in their surroundings. Because the former is a singular solution of the Einstein equations and the latter is not, the existence of the *Innermost Stable Circular Orbit* (ISCO) becomes manifested. Due to the regularity of the central object in the RAR case, there is no critical angular momentum of the particle for which a potential barrier is no longer present, and therefore no ISCO can be reached (Crespi 2022). This behaviour directly implies that there is no clear inner boundary as to where the disc might extend². To set an inner constraint in this regard, we study the binding energy of a test particle in the disc, and analyse when it saturates towards a maximum.

² General Relativistic simulations of fluid dynamics should be performed to tackle this problem in analogy to boson stars either for unmagnetised (Meliani et al. 2016) or magnetised scenarios (Olivares et al. 2020), though both are out of the scope of this paper.

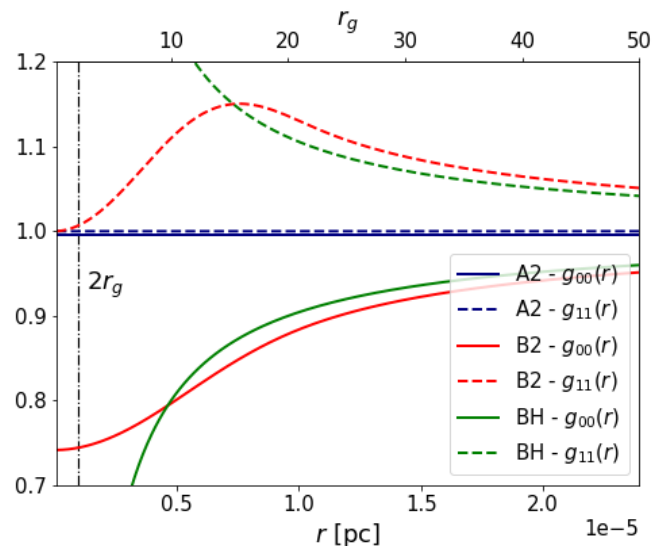


Fig. 3: Metric components corresponding to the same RAR solutions as in Fig. 2 with core mass of $M_c = 10^7 M_\odot$, and particle masses of $mc^2 = 48$ keV (A2, blue) and $mc^2 = 200$ keV (B2, red). A comparison with the metric of a Schwarzschild BH of mass $M_{BH} = 10^7 M_\odot$ is also shown (BH, green).

In the case of BHs, the efficiency of the accretion process is related to the binding energy per unit rest mass at the innermost stable circular orbit (ISCO), that is:

$$\varepsilon = \frac{mc^2 - E_c}{mc^2} \quad (8)$$

where E_c corresponds to the particle's energy at the last stable circular orbit. This accretion efficiency represents the maximum fraction of the rest mass energy of the accreted particle that can be converted into radiated energy. In standard astrophysical scenarios such as a neutron star of radius ~ 10 km, the efficiency is of order 10%, while in the case of BH accretion the efficiency varies between 5.7% and 42% for Schwarzschild and Kerr (maximal rotation with prograde disc) solutions respectively³ (Novikov & Thorne 1973). In analogy to the BH case, and in order to define the corresponding accretion efficiency in the RAR model, we seek for a maximum in the radial behaviour of the (normalised) binding energy of a test particle. Thus, in the RAR-solution, the binding energy normalised with the rest mass reads:

$$\bar{E}_b(r) = 1 - \sqrt{g_{00}(r) \left(1 + \frac{rg'_{00}(r)}{2g_{00}(r) - rg'_{00}(r)} \right)}. \quad (9)$$

where $g_{00}(r) = e^{\nu(r)}$ is the temporal component of the metric, and the prime symbol indicates derivation with respect to r . We show this binding energy behaviour in Fig. 4 for the case of a Schwarzschild BH -obtained by replacing $g_{00}(r)$ in Eq. 9 by $1 - 2GM/r$, and for two different RAR solutions with the

³ When considering the effects of the radiation of the disc into the rotation of the black hole, the maximum spin reduces, and the efficiency results in 32.4% (Thorne 1974; Laor & Netzer 1989).

Table 1: Main parameters of the different RAR models.

Model	Particle mass [keV]	M_c [M_\odot]	M_{tot} [$10^{11}M_\odot$]	r_c [r_g]	θ_0	W_0	β_0
A1	48	1.5×10^6	3	1.5×10^4	39.5	69.6	2.5×10^{-6}
A2	48	1.0×10^7	10	1.0×10^3	37.9	66.6	6.8×10^{-5}
A3	48	1.2×10^8	45	3.4×10^1	38.8	67.2	1.1×10^{-3}
B1	200	3.5×10^6	3	8.1×10^1	49.4	77.9	5.1×10^{-3}
B2	200	1.0×10^7	10	1.5×10^1	44.3	75.4	2.1×10^{-3}

same DM core mass of $M_c = M_{\text{BH}} = 10^7 M_\odot$ but different core-compacities. For the RAR solutions the binding energy asymptotically reaches the maximum as $r \rightarrow 0$, and saturates (see definition below) at a given radius r_{in} . The definition for r_{in} implies that it is always smaller than the core radius, with the binding energy remaining approximately constant as the particle's orbit gets smaller and smaller (i.e. until $r_{\text{min}} \sim 10^{-7} r_g \approx 10^{-13}$ pc, the smallest representable radius admitted by computer precision for such *core-halo* solutions). We adopt as the inner radius of the disc, r_{in} , the value at which the relative error for the change in the maximum efficiency of the binding energy is equal or lower than 1%, that is:

$$\frac{|\bar{E}_b(r_{\text{in}}) - \bar{E}_b(r_{\text{min}})|}{\bar{E}_b(r_{\text{min}})} \leq 0.01 \quad (10)$$

Adopting this definition, the inner radius corresponds typically to a tenth of the core radius $r_{\text{in}} \sim 0.1 r_c$ (for 1% of relative error). We compare the efficiencies of the RAR models A_2 and B_2 (labelled with ϵ_{A2} and ϵ_{B2} in Fig. 4), with the Schwarzschild one labelled with ϵ_{BH} . Remarkably, since the disc can enter deep inside the DM core (that is the Keplerian orbits in the disc can have $r < r_c$), the binding energy of RAR solutions with compact enough cores can surpass the maximum Schwarzschild value. In Fig. 4 we show an example for a below-critical DM core (solution B_2) with an efficiency of 14%, to be compared with the 5.7% of the BH case. Moreover, when the degenerate core achieves its critical mass of collapse the accretion efficiency can be as large as $\approx 28\%$, similar to highly rotating Kerr BH. This interesting result is not new, and analogous conclusions were already obtained in the past for relativistic clusters with constant density and different compacities by (Cocco et al. 1995).

These novel conclusions, exemplified in Fig. 4, have potential implications in the astrophysics of AGNs. In the context of the Soltan argument (Soltan 1982), and based on observational results about the mean accretion efficiency of SMBHs (both from the local and the AGN-relic Universe, Yu & Tremaine 2002; Ueda et al. 2003; Marconi et al. 2004), it arises a mean value of $\epsilon \approx 0.1$ falling between the one predicted by the Schwarzschild and Kerr BH cases. Additionally, data analysis of different populations of AGNs shows that required efficiencies are $\epsilon > 0.1$ (Raimundo & Fabian 2009), with the bulk of the cases having $\epsilon \sim 0.2-0.3$ and a minority of them reaching even down to 0.04 (such a lower value compatible with (Marconi et al. 2004)). Given these values, the relevance of the results here presented for the accretion efficiencies onto the compact DM cores becomes clear: depending on the compacity of the fermion core, the efficiency can go from below the typical Schwarzschild case up to values larger than 0.1, typical of Kerr BHs, as preferred by AGN population analysis. Further discussions about the challenges to observationally confirm the Kerr BH space-time at galaxy centers, mainly related to degeneracy of models regarding the mass

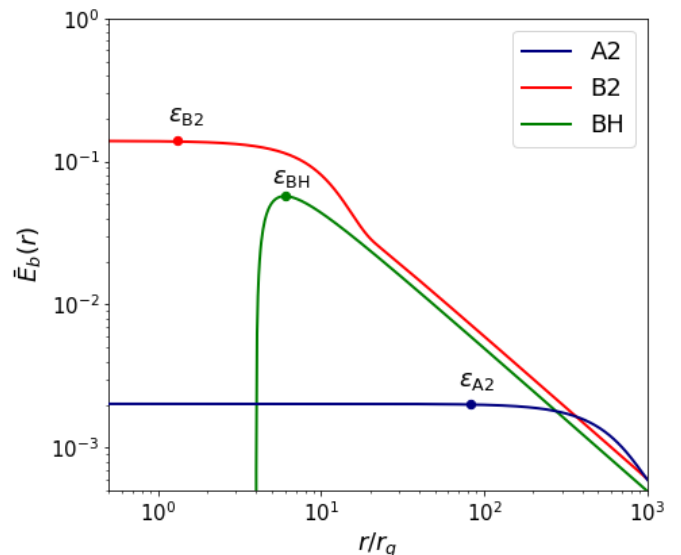


Fig. 4: Accretion efficiencies (labelled with coloured dots) for two different DM core compacities (i.e. different m) having the same core mass of $M_c = 10^7 M_\odot$ (RAR solutions A_2 and B_2). For comparison, the case of a Schwarzschild BH with a mass equal to M_c is also shown. Interestingly, solution B_2 reaches an accretion efficiency of 14%, considerably larger than that of the Schwarzschild BH.

of the compact object and, in particular, the spin parameter and possible deviations from the Kerr metric, can be found in Bambi (2017).

3.2. The steady standard disc model embedded in DM

In this section we consider the model of steady thin discs developed by Shakura & Sunyaev (Shakura & Sunyaev 1973), and extend it to be applied in the context of the RAR-solutions. To this end, and following the treatment presented in Frank et al. (2002), we use cylindrical polar coordinates (r, ϕ, z) , and assume that matter is very close to the plane $z = 0$, and it is rotating with an angular velocity $\Omega(r)$ that remains very close to the Keplerian value:

$$\Omega = \Omega_K(r) = \left(\frac{GM(r)}{r^3} \right)^{1/2}. \quad (11)$$

Here, $M(r)$ is the mass distribution of the DM *core-halo* solution contained up to r . The circular velocity is given by $v_\phi = r\Omega_K(r)$.

In addition, the gas is assumed to possess a small radial ‘drift’ velocity $v_R(r)$, which is negative near the central object,

Table 2: r_{in} considered for the different models.

Model	Particle mass [keV]	M_c [M_\odot]	r_c [r_g]	r_{in} [r_g]	ε [%]
A1	48	1.5×10^6	1.5×10^4	9.6×10^2	0.02
A2	48	1.0×10^7	1.0×10^3	8.3×10^1	0.2
A3	48	1.2×10^8	3.4×10^1	2.6×10^0	6.7
B1	200	3.5×10^6	8.1×10^1	6.8×10^0	2.5
B2	200	1.0×10^7	1.5×10^1	1.3×10^0	14

so that matter is being accreted. The disc is characterised by its surface density $\Sigma(r)$, which is the mass per unit surface area of the disc, given by integrating the gas density ρ in the z -direction. For a steady disc, the conservation of mass and angular momentum can be written as:

$$\dot{M} = 2\pi r \Sigma(-v_R), \quad (12)$$

$$\eta \Sigma = \frac{\dot{M}}{3\pi} \left[1 - \left(\frac{M_{\text{in}} r_{\text{in}}}{M(r)r} \right)^{1/2} \right] \left[1 - \frac{r}{3M(r)} \frac{dM(r)}{dr} \right]^{-1}, \quad (13)$$

respectively. Here, \dot{M} is the accretion rate (in units of g s^{-1}), η is the cinematic viscosity, r_{in} is the internal radius of the disc (see section 3.1), and $M_{\text{in}} = M(r_{\text{in}})$.

Analogously as in the BH case, we adopt the viscous torques to vanish at the maximum of the binding energy, which in the case of the RAR model correspond to the inner radius r_{in} . Thus it allows to explicitly obtain the viscous dissipation per unit disc face area as:

$$D(r) = \frac{1}{2} \eta \Sigma \left(r \frac{d\Omega}{dr} \right)^2 = \frac{3\dot{M}}{8\pi} \frac{GM(r)}{r^3} \left[1 - \left(\frac{M_{\text{in}} r_{\text{in}}}{M(r)r} \right)^{1/2} \right] \left[1 - \frac{r}{3M(r)} \frac{dM(r)}{dr} \right]. \quad (14)$$

It can be seen that, as in the standard solution, the viscous dissipation is independent of the physical nature of the viscosity η . Finally, the total disc luminosity is obtained by integrating $D(r)$ along the disc area.

We also consider an optically thick disc in the z -direction, hence each element of the disc radiates as a black-body with temperature $T(r)$, given by the equation of the viscous dissipation per unit disc face area $D(r) = \sigma T^4(r)$, with σ the Stefan-Boltzmann constant. In Fig. 5 we show the comparison between the A and B RAR models, with a BH of $M \sim 10^7 M_\odot$.

For an observer at a distance d from the centre of the disc whose line of sight makes an angle i with respect to the normal of the disc plane, the flux at frequency ν is:

$$F_\nu = \frac{4\pi h \cos i \nu^3}{c^2 d^2} \int_{r_{\text{in}}}^{r_{\text{out}}} \frac{r dr}{e^{h\nu/kT(r)} - 1}. \quad (15)$$

The outer radius r_{out} can be estimated using the condition that the disc becomes locally self-gravitating [Bogdán & Goulding \(2015\)](#). This is determined by analysing the stability criterion for a differential rotation disc:

$$Q_T = c_s \Omega / \pi G \Sigma \gg 1, \quad (16)$$

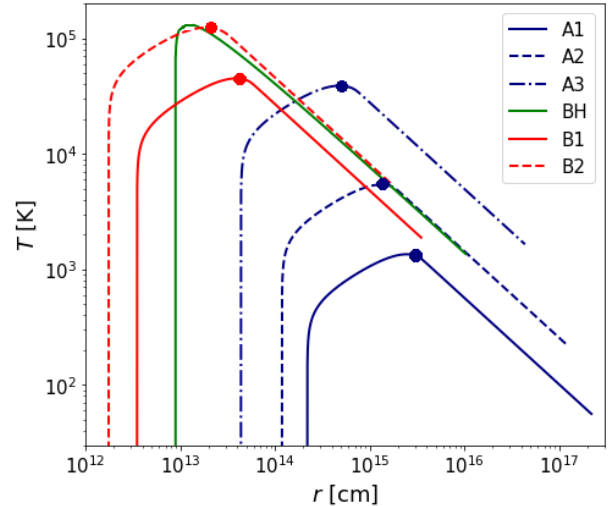


Fig. 5: Comparison of disc temperatures for the A and B RAR models with that of a BH of mass $M_{\text{BH}} \sim 10^7 M_\odot$. The dots indicate the location of the R_c for each RAR model.

where Ω is the angular velocity given in Eq. 11. The condition $Q_T = 1$ defines the self-gravitating disc:

$$r_{\text{out}} = (M/\pi\rho)^{1/3}. \quad (17)$$

Knowing the density of the accretion disc, the outer radius can be determined. Further details are discussed in Appendix A, where we obtained $r_{\text{out}} \approx 10^3 r_g - 10^4 r_g$, depending on the model studied. Nevertheless, the disc beyond $10^3 r_g$ does not contribute significantly to the total luminosity, hence we adopt this value as the outer limit for all models.

In Fig. 6 we show the luminosities obtained for models A and B. In all cases we have considered $\dot{M} = 0.1 \dot{M}_{\text{Edd}}$, where \dot{M}_{Edd} is the Eddington accretion rate, defined as the accretion rate at which the compact source radiates at an efficiency of $\varepsilon \sim 0.1$ of the Eddington luminosity, that is $\dot{M}_{\text{Edd}} = L_{\text{Edd}}/\varepsilon c^2 \sim 1.4 \times 10^{16} (M_c/M_\odot) \text{ erg s}^{-1}$. Moreover, we show the comparison with a black hole of $M \sim 10^7 M_\odot$. See also points (ii) and (iii) in Section 4 for a relevant discussion regarding the RAR model predictions for disc luminosities.

Figure 7 only shows the luminosity for RAR models with $M_c = 10^7 M_\odot$, using two values for the fermion mass: $mc^2 = 48 \text{ keV}$ (model A2) and $mc^2 = 200 \text{ keV}$ (model B2); we also compare this result with a disc around a Schwarzschild black hole of $M_{\text{BH}} = M_c$. This important result shows that it exist a core compacity (i.e. solution B2) for which the luminosity spectrum is basically indistinguishable from that of a Schwarzschild BH of the same mass as the DM core.

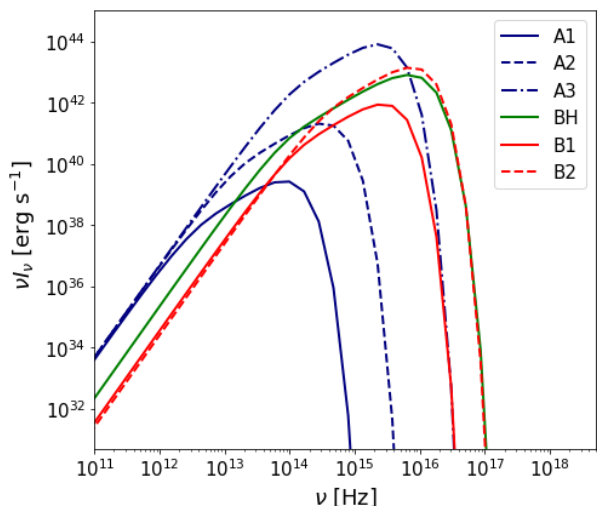


Fig. 6: Comparison of the luminosity for the A and B models with a BH of $M \sim 10^7 M_\odot$. The larger the mass of the DM-core, the more compact and dense is the degenerate core, implying the luminosity peak shifts towards higher ν .

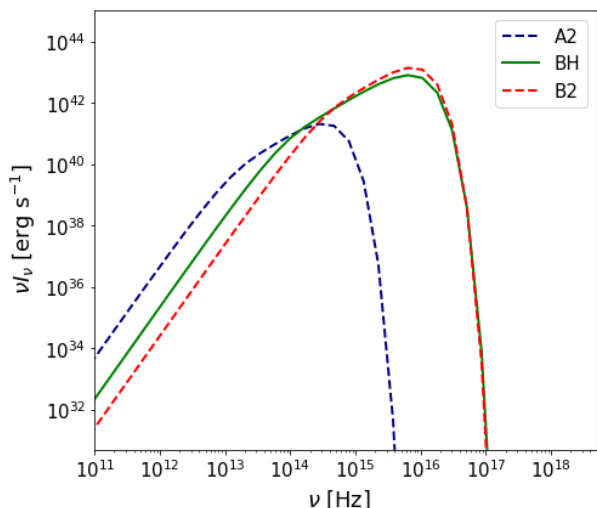


Fig. 7: Comparison of luminosity for the A2, B2 models and a BH of $\sim 10^7 M_\odot$. Thus it exist a specific core compacity which produces a luminosity spectrum which is basically indistinguishable from that of a BH of the same mass as the DM core.

Different hypothesis are behind the standard thin disc approximation: the azimuthal velocity v_ϕ remains close to the Keplerian value, the disc remains thin at all radii, i.e. the height scale H is much smaller than the extent of the disc $H \ll r$, and the disc is optically thick in the z -direction. In order to corroborate if the solutions here obtained for the RAR model are consistent with the above thin disc ansatz, we consider a disc in hydrostatic equilibrium in the z -direction, meaning that there is no flow in the vertical direction. Then, for $H \ll r$ and $P \approx \rho c_s^2$ (with c_s the sound speed), the solution satisfies:

$$c_s \ll \left(\frac{GM(r)}{r} + G \frac{dM(r)}{dr} \right)^{1/2} \approx \left(\frac{GM(r)}{r} \right)^{1/2}. \quad (18)$$

The local standard Kepler velocity should be highly supersonic.

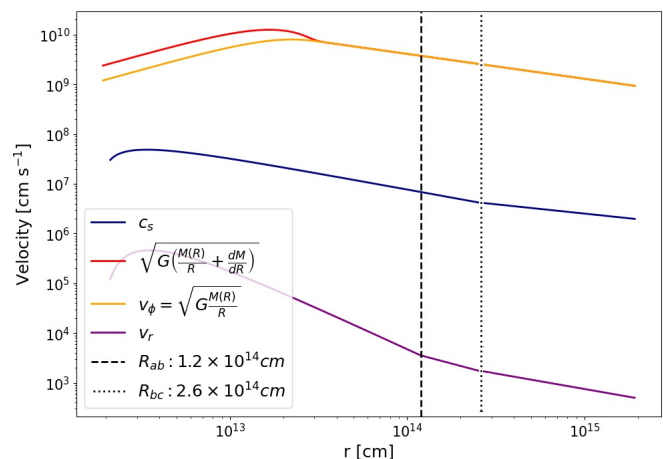


Fig. 8: Hypothesis validation for model A2: Keplerian velocity must be highly supersonic, while radial velocity must be highly subsonic. Vertical dashed (and dotted) lines specify R_{ab} (and R_{bc}), i.e. the radii at which the behaviour of the disc changes between the inner and intermediate region (and between the intermediate and outer region) respectively (see Appendix A.)

If the thin disc condition in Eq. 18 holds, the circular matter velocity v_ϕ satisfies

$$v_\phi = \sqrt{\frac{GM(r)}{r} + G \frac{dM(r)}{dr}} [1 + O(M^{-2})]. \quad (19)$$

It can be seen that v_ϕ is very close to the Keplerian value, as we have assumed. Figure 8 shows both hypothesis for model A2 as an example, though it is satisfied by all solutions as we have verified.

At this point it is worth to emphasise that the complete structure of the disc was not needed in order to compute the spectra for the RAR solutions. However, in order to be able to verify the hypothesis above mentioned, in Appendix A we write down the generalisation of the Shakura & Sunyaev set of equations within the fermionic DM model, and solve for the complete disc structure within the α prescription for the viscosity (see Frank et al. (2002) for the analogous demonstration in the case of the standard α disc theory).

4. Discussion and final remarks

We have extended the standard steady thin disc model in order to study the accretion onto horizonless dark compact objects at galaxy centres. The BH alternative here investigated consists in a dense and highly degenerate core made of neutral fermions, surrounded by a more diluted mass distribution that is able to explain the DM halo in galaxies. Such a *dense core–diluted halo* DM configuration is known as the RAR model, and is a non-analytic solution of the Einstein equations of GR, which naturally arises once the quantum nature (i.e. Pauli principle) of the fermions is fully accounted for. The attention in this work was centred in active-like galaxies together with their central accretion processes, luminosity spectra and efficiencies.

We have used core-halo RAR solutions for two different fermion masses, 48 keV and 200 keV, the later corresponding to a very dense DM-core of mass $10^7 M_\odot$, close to its critical value of gravitational collapse to a BH. The fact that the larger

m the more compact is the DM-core of given mass (see Fig. 2), makes the above choice particularly relevant to analyse how similar to a BH the luminosity spectra of α -discs can be. Moreover, a particle mass falling within this range is totally compatible with both, linear structure formation in cosmology as well as non-linear structure formation, including galaxy rotation curves and scaling relations (see Argüelles et al. (2023a) for a review and references therein).

The main results of our work can be summarised as follows:

1. The fact that the dense DM core is transparent implies the accretion disc can enter inside reaching down to event-horizon scales. As a consequence, it can achieve accretion efficiencies as large as $\epsilon = 28.5\%$ and thus comparable to that of a highly rotating Kerr BH. In Fig. 4 we have shown a relevant example comparing a $10^7 M_\odot$ Schwarzschild BH with two different RAR solutions of increasing particle mass (A_2 and B_2) having the same core mass. It is shown that for $m = 48$ keV (solution A_2) the efficiency is below 1% while for $m = 200$ keV (solution B_2) the stable (i.e. below critical) DM core is compact enough so to reach, at $r_{in} < r_c$, an accretion efficiency which is more than two times that of the BH. The maximum efficiency of $\epsilon = 28.5\%$ is achieved for the critical core mass. The relevance of achieving Kerr-like efficiencies in active galaxies is supported by observational results (Raimundo & Fabian 2009) based on the Soltan argument.
2. At given DM core mass M_c , the larger the particle mass the more compact is the degenerate core, and consequently the more luminous and energetic are the discs. This result, when considered in light of the efficiency trend explained above, implies it always exist a given core compacity producing a luminosity spectrum which is almost indistinguishable from that of a Schwarzschild BH of the same mass as the DM core. This important RAR model prediction is explicitly shown in Fig. 7 for a BH mass of $10^7 M_\odot$ typical of an active galaxy.
3. At fixed DM particle mass it is possible to have different DM core masses M_c (see Table 1) with surrounding DM halos fulfilling with the observationally inferred Ferrarese scaling relation Ferrarese (2002) (see Fig. 1 and Argüelles et al. (2019)). A novel RAR model prediction found in this work is that when M_c increases, the peak frequency of the luminosity spectra also increases (see e.g. the trend in the red curves B_1 and B_2 of Fig. 6). This is due to the degeneracy of the core, which implies more compact solutions for more massive cores (at given m). This results is opposite to what is expected from accretion into a BH, and could be a fundamental tool to test the RAR model (see discussion below).

Further detailed work is needed when trying to differentiate both paradigms of supermassive compact objects, as for example making use of real spectral energy distributions (SED) of AGNs, or to calculate the relativistic images produced by the emitted photons via ray tracing techniques. The later is an important project already started by our team, which will allow us to contrast with observations the shadow-like features predicted by the RAR model in contrast with the ones predicted by the BH.

Regarding the observational access to SEDs of AGNs relative to this work, the most important is the narrow window of low central object masses $\sim 10^6$ - $10^7 M_\odot$ (for the $m = 200$ keV case), or $\sim 10^7$ - $10^8 M_\odot$ (for $m = 48$ keV), before the corresponding DM core becomes critical and collapses to a BH⁴. An eventual

observational detection of luminosity peaks which shifts towards higher ν in such a small DM core-mass window is challenging. This is mainly because of the lack of data in the UV band (at about the UV bump) due to the absorption of the IGM; the large error bars at about the blue bump; or that most of observed SEDs are obtained for relatively large central object masses $> 10^8 M_\odot$ (Collinson et al. 2017).

All in all, the original results presented in this work and summarised above may imply an important landmark -and may open new avenues of research- in the field of AGN theory and phenomenology in connection to DM physics and SMBHs.

Acknowledgements. C.R.A. acknowledges supported from CONICET of Argentina, the ANPCyT (grant PICT-2018-03743), and ICRANet. F.L.V. acknowledges support from the Argentine agency CONICET (PIP 2021-0554). V.C. thanks financial support from CONICET, Argentina. MFM acknowledges support from CONICET (PIP2169) and from the Universidad Nacional de La Plata (G168).

References

- Akiyama, K., Alberdi, A., Alef, W., et al. 2022, ApJ, 930, L13
 Alberti, G. & Chavanis, P.-H. 2020, European Physical Journal B, 93, 208
 Argüelles, C. R., Becerra-Vergara, E. A., Krut, A., et al. 2022a, International Journal of Modern Physics D, 31, 2230002
 Argüelles, C. R., Becerra-Vergara, E. A., et al. 2023a, Universe, 9, 197
 Argüelles, C. R., Boshkayev, K., Krut, A., et al. 2023b, MNRAS, 523, 2209
 Argüelles, C. R., Díaz, M. I., Krut, A., & Yunis, R. 2021, MNRAS, 502, 4227
 Argüelles, C. R., Krut, A., Rueda, J. A., & Ruffini, R. 2018, Physics of the Dark Universe, 21, 82
 Argüelles, C. R., Krut, A., Rueda, J. A., & Ruffini, R. 2019, Physics of the Dark Universe, 24, 100278
 Argüelles, C. R., Mestre, M. F., Becerra-Vergara, E. A., et al. 2022b, MNRAS, 511, L35
 Argüelles, C. R., Mestre, M. F., Becerra-Vergara, E. A., et al. 2022c, MNRAS, 511, L35
 Argüelles, C. R., Rueda, J. A., & Ruffini, R. 2023, arXiv e-prints, arXiv:2312.07461
 Argüelles, C. R. & Ruffini, R. 2014, International Journal of Modern Physics D, 23, 1442020
 Bahcall, N. A., Ostriker, J. P., et al. 1999, Science, 284, 1481
 Bambi, C. 2017, Reviews of Modern Physics, 89, 025001
 Battaglia, G., Helmi, A., Tolstoy, E., et al. 2008, ApJ, 681, L13
 Becerra-Vergara, E. A., Argüelles, C. R., Krut, A., et al. 2020, A&A, 641, A34
 Becerra-Vergara, E. A., Argüelles, C. R., et al. 2021, MNRAS, 505, L64
 Bilic, N., Munyaneza, F., Tupper, G. B., & Viollier, R. D. 2002, Progress in Particle and Nuclear Physics, 48, 291
 Bogdán, A. & Goulding, A. D. 2015, ApJ, 800, 124
 Bozek, B., Fitts, A., Boylan-Kolchin, M., et al. 2019, MNRAS, 483, 4086
 Bullock, J. S. & Boylan-Kolchin, M. 2017, ARA&A, 55, 343
 Cardoso, V. & Pani, P. 2019, Living Reviews in Relativity, 22, 4
 Chau, W. Y., Lake, K., & Stone, J. 1984, ApJ, 281, 560
 Chavanis, P.-H. 2004, Physica A Statistical Mechanics and its Applications, 332, 89
 Chavanis, P. H. 2006, International Journal of Modern Physics B, 20, 3113
 Chavanis, P.-H. 2022, Phys. Rev. D, 106, 043538
 Chavanis, P.-H. & Alberti, G. 2019, arXiv e-prints, arXiv:1908.10303
 Chavanis, P.-H., Lemou, M., & Méhats, F. 2015, Phys. Rev. D, 92, 123527
 Chavanis, P. H. & Sommeria, J. 1998, MNRAS, 296, 569
 Cocco, V., Pascale, E., & Ruffini, R. 1995, Nuovo Cimento B Serie, 110B, 95
 Collaboration, E. H. T., Akiyama, K., Alberdi, A., et al. 2019, ApJ, 875, L1
 Collinson, J. S., Ward, M. J., Landt, H., et al. 2017, MNRAS, 465, 358
 Crespi, V. 2022, M.sc. thesis, UNLP. Available at [SIDECI](#)
 Destri, C., de Vega, H. J., & Sanchez, N. G. 2013, New A, 22, 39
 Diemand, J., Zemp, M., Moore, B., Stadel, J., et al. 2005, MNRAS, 364, 665
 Donato, F., Gentile, G., Salucci, P., et al. 2009, MNRAS, 397, 1169
 Ferrarese, L. 2002, ApJ, 578, 90
 Frank, J., King, A., & Raine, D. J. 2002, Accretion Power in Astrophysics: Third Edition
 Gao, J. G., Merafina, M., & Ruffini, R. 1990, A&A, 235, 1
 Genzel, R., Eisenhauer, F., & Gillessen, S. 2010, Rev. Mod. Phys., 82, 3121
 Ghez, A. M., Salim, S., Hornstein, S. D., et al. 2005, ApJ, 620, 744
 Ghez, A. M., Salim, S., Weinberg, N. N., et al. 2008, ApJ, 689, 1044
 Gravity Collaboration, Abuter, R., Amorim, A., et al. 2018, A&A, 618, L10
 Guzmán, F. S. 2006, Phys. Rev. D, 73, 021501
 Ingrassio, G. & Ruffini, R. 1988, Nuovo Cimento B Serie, 101, 369

- Ivanov, M. M., Simonović, M., et al. 2020, *Phys. Rev. D*, 101, 083504
- Joung, M. R., Cen, R., & Bryan, G. L. 2009, *ApJ*, 692, L1
- Kaplinghat, M., Ren, T., et al. 2020, *J. Cosmology Astropart. Phys.*, 2020, 027
- Krut, A., Argüelles, C. R., Chavanis, P. H., et al. 2023, *ApJ*, 945, 1
- Laor, A. & Netzer, H. 1989, *MNRAS*, 238, 897
- Lynden-Bell, D. 1967, *MNRAS*, 136, 101
- Marconi, A., Risaliti, G., Gilli, R., et al. 2004, *MNRAS*, 351, 169
- McGaugh, S. S., Lelli, F., et al. 2016, *Phys. Rev. Lett.*, 117, 201101
- Meliani, Z., Grandclément, P., Casse, F., et al. 2016, *Classical and Quantum Gravity*, 33, 155010
- Novikov, I. D. & Thorne, K. S. 1973, in *Black Holes (Les Astres Occlus)*, ed. C. Dewitt & B. S. Dewitt, 343–450
- Olivares, H., Younsi, Z., Fromm, C. M., et al. 2020, *MNRAS*, 497, 521
- Oppenheimer, J. R. & Volkoff, G. M. 1939, *Physical Review*, 55, 374
- Raimundo, S. I. & Fabian, A. C. 2009, *MNRAS*, 396, 1217
- Ruffini, R., Argüelles, C. R., & Rueda, J. A. 2015, *MNRAS*, 451, 622
- Schive, H.-Y., Chiueh, T., & Broadhurst, T. 2014, *Nature Physics*, 10, 496
- Schunck, F. E. & Mielke, E. W. 1999, *GR and Gravitation*, 31, 787
- Shakura, N. I. & Sunyaev, R. A. 1973, *A&A*, 24, 337
- Soltan, A. 1982, *MNRAS*, 200, 115
- Thorne, K. S. 1974, *ApJ*, 191, 507
- Torres, D. F., Capozziello, S., & Lambiase, G. 2000, *Phys. Rev. D*, 62, 104012
- Ueda, Y., Akiyama, M., Ohta, K., & Miyaji, T. 2003, *ApJ*, 598, 886
- Vincent, F. H., Meliani, Z., Grandclément, P., Gourgoulhon, E., & Straub, O. 2016, *Classical and Quantum Gravity*, 33, 105015
- Yu, Q. & Tremaine, S. 2002, *MNRAS*, 335, 965

Appendix A: Local structure of the disc

We present here the solution of the complete disc structure. To this end, we consider, as in the standard disc solution, the α -prescription for the viscosity, given by:

$$\eta = \alpha c_s H. \quad (\text{A.1})$$

The main objective of the following theoretical content of this Appendix is done both, for completeness, and in order to be able to verify the three main hypothesis of the (extended) Shakura & Sunyaev theory: the geometrically thin disc ($H(r) \ll r$) and the Keplerian velocity approximation, together with the optically thick ($\tau > 1$) assumption, for which the solution of the full disc structure is needed. An example of such a verification was shown in Fig. 8 of the main text.

In the thin disc approximation, the determination of the disc structure is simplified. Following Shakura & Sunyaev (1973); Frank et al. (2002), and using the results obtained in Section 3.2 for the generalised thin disc embedded within the RAR DM distribution, the set of disc equations results in:

1. $\rho = \Sigma/H$,
2. $H = c_s \left(\frac{GM(r)}{r} + G \frac{dM(r)}{dr} \right)^{-1/2} r$,
3. $c_s^2 = P/\rho$,
4. $P = \frac{\rho(r)kT_c}{\mu m_p} + \frac{4\sigma}{3c} T_c^4$,
5. $\frac{4\sigma T_c^4}{3\tau} = \frac{3\dot{M}}{8\pi} \frac{GM(r)}{r^3} \left[1 - \left(\frac{M_{\text{in}} r_{\text{in}}}{M(r)r} \right)^{1/2} \right] \left(1 - \frac{r}{3M(r)} \frac{dM(r)}{dr} \right)$,
6. $\tau = \Sigma \kappa_R(\rho, T_c) = \tau(\Sigma, \rho, T_c)$,
7. $\eta \Sigma = \frac{\dot{M}}{3\pi} \left[1 - \left(\frac{M_{\text{in}} r_{\text{in}}}{M(r)r} \right)^{1/2} \right] \frac{1}{1 - \frac{r}{3M(r)} \frac{dM(r)}{dr}}$,
8. $\eta = \eta(\rho, T_c, \Sigma, \alpha, \dots)$.

It is worth mentioning that in the limits $M(r) \rightarrow M$ and $\frac{dM(r)}{dr} \rightarrow 0$, the standard disc solutions are recovered.

There are three distinct regions in the disc, determined by the relevant absorption mechanism, and the importance of P_{rad} versus P_{gas} . Regarding the absorption mechanisms, we consider two main processes: free-free absorption, where the opacity is given by (see e.g. Shakura & Sunyaev (1973))

$$\kappa_{\text{ff}} = 5.0 \times 10^{24} \rho T_c^{-7/2} \text{ cm}^2 \text{ g}^{-1}, \quad (\text{A.2})$$

and scattering, where we adopt:

$$\kappa_{\text{sc}} = \frac{\sigma_T}{m_p} \sim 0.4 \text{ cm}^2 \text{ g}^{-1}. \quad (\text{A.3})$$

The parameterization of the complete solutions, together with the regions where P_{gas} dominates over P_{rad} (and vice versa) can be found in Appendix A.

As in the standard solution, there are three distinct regions in the disc: (a) an inner region, where $P_{\text{rad}} \gg P_{\text{gas}}$ and $\kappa_{es} \gg \kappa_{ff}$, (b) an intermediate region, where $P_{\text{gas}} \gg P_{\text{rad}}$ and $\kappa_{es} \gg \kappa_{ff}$, and (c) an outer region, where $P_{\text{gas}} \gg P_{\text{rad}}$ and $\kappa_{es} \ll \kappa_{ff}$. The complete solution of the set of Eqs. 1-8 for the inner, intermediate and outer region are presented in Eqs. A.7-A.9, A.14-A.19 and A.20-A.26, respectively. We have defined $R_{10} = r/(10^{10} \text{ cm})$, $m_1 = M(r)/M_\odot$, $\dot{M}_{16} = \dot{M}/(10^{16} \text{ g s}^{-1})$, $f^4 = 1 - \left(\frac{M_{\text{in}} r_{\text{in}}}{M(r)r} \right)^{1/2}$, $A = \left(\frac{M(r)}{r} + \frac{dM}{dr} \right)$, $B = 1 - \frac{r}{3M(r)} \frac{dM(r)}{dr}$ and we have considered $\mu = 0.615$ for a fully ionised gas.

It is worth noticing that the limits $\frac{dm_1}{dR_{10}} \rightarrow 0$ and $M(r) \rightarrow M_{\text{in}}$ recover the standard disc solution around a compact object of given mass M . Secondly, the α power is of the same order of

magnitude than that of the standard solution. Hence, as α powers are low, the magnitudes calculated for the disc are not sensitive to the value of α .

The transition radii between the regions result in:

$$R_{ab} \approx 3.9 \times 10^7 \alpha^{1/16} m_1^{1/2} f^2 \dot{M}_{16}^{1/2} B^{1/2} A^{-11/32} \text{ cm}, \quad (\text{A.4})$$

$$R_{bc} \approx 2.2 \times 10^5 m_1^{1/2} f^2 \dot{M}_{16}^{1/2} B^{1/2} A^{-1/4} \text{ cm} \quad (\text{A.5})$$

We now consider the case of models A2 and B2 described in Table 1. We assume $\dot{M} = 0.1 \dot{M}_{\text{Edd}} \approx 1.4 \times 10^{23} \text{ g s}^{-1}$, and $\alpha = 0.1$. We also compare to the standard disc around a Schwarzschild black hole of mass $M_{\text{BH}} = 10^7 M_\odot$.

In Fig. A.1 we show the variation of both contributions to the total pressure in the different regions; in an analogous way, in Fig. A.2 we show the absorption coefficients due to scattering and free-free absorption. In both cases, we have compared our models (centre and right) to the standard disc around a black hole (left).

An interesting result is obtained varying the fermion mass from 200 keV to 48 keV (for the same mass of the core, model A2); in this case, only the outer region exists. This is due to the fact that the compacity of the core diminish for lower masses of the fermion, which leads the disc to reach lower temperatures, as it can be seen in Fig. 5.

Using the criterion given by Eq. 17, we can determined the outer radius of the disc. For both, model B2 and the black hole, $r_{\text{out}} = 1.9 \times 10^{15} \text{ cm}$ and $r_{\text{out}} = 1.0 \times 10^{14} \text{ cm}$, respectively, which implies for both cases $r_{\text{out}} \approx 10^3 r_g$. It is interesting to analyse model A2, where only the outer region of the disc is present. In this case, we found that the disc becomes self-gravitating at $r_{\text{out}} = 1.3 \times 10^{16} \text{ cm} \approx 10^4 r_g$.

Inner region of the disc: $P_{\text{rad}} \gg P_{\text{gas}}$ and $\kappa_{es} \gg \kappa_{ff}$:

$$\Sigma = 5.0 \times 10^8 \alpha^{-4/5} f^{12/5} B^{-2} A m_1^{1/5} \dot{M}_{16}^{3/5} R_{10}^{-3/5} \text{ g cm}^{-2}; \quad (\text{A.6})$$

$$H = 1.4 \times 10^4 m_1^{-7/20} R_{10}^{21/20} \dot{M}_{16}^{1/5} f^{4/5} \text{ cm}; \quad (\text{A.7})$$

$$\rho = 3.7 \times 10^4 \alpha^{-4/5} f^{8/5} B^{-2} A m_1^{11/20} \dot{M}_{16}^{2/5} R_{10}^{-33/20} \text{ g cm}^{-3}; \quad (\text{A.8})$$

$$T_c = 7.7 \times 10^5 \alpha^{-1/5} m_1^{3/10} B^{-1/2} A^{1/4} R_{10}^{-9/10} \dot{M}_{16}^{2/5} f^{8/5} \text{ K}; \quad (\text{A.9})$$

$$\tau = 2.3 \times 10^{17} \alpha^{-4/5} f^{12/5} B^{-2} A m_1^{1/5} \dot{M}_{16}^{3/5} R_{10}^{-3/5}; \quad (\text{A.10})$$

$$\eta = 9.4 \times 10^7 \alpha m_1^{13/20} A^{-1/2} R_{10}^{-19/20} \dot{M}_{16}^{2/5} f^{24/5} \text{ cm}^2 \text{ s}^{-1}; \quad (\text{A.11})$$

$$v_R = 9.4 \times 10^{-3} m_1^{13/20} A^{-1/2} R_{10}^{-39/20} \dot{M}_{16}^{2/5} f^{24/5} \text{ cm s}^{-1}. \quad (\text{A.12})$$

Intermediate region: $P_{\text{gas}} \gg P_{\text{rad}}$ and $\kappa_{es} \gg \kappa_{ff}$:

$$\Sigma = 9.9 \alpha^{-4/5} f^{12/5} m_1^{-1/5} \dot{M}_{16}^{3/5} R_{10}^{-1/5} A^{2/5} B^{-1} \text{ g cm}^{-2}; \quad (\text{A.13})$$

$$H = 9.6 \times 10^7 \alpha^{-1/10} m_1^{1/10} \dot{M}_{16}^{1/5} R_{10}^{3/5} f^{4/5} A^{-9/20} \text{ cm}; \quad (\text{A.14})$$

$$\rho = 1.0 \times 10^{-7} \alpha^{-7/10} m_1^{-3/10} \dot{M}_{16}^{2/5} R_{10}^{-4/5} f^{8/5} A^{13/20} B^{-1} \text{ g cm}^{-3}; \quad (\text{A.15})$$

$$T_c = 9.2 \times 10^3 \alpha^{-1/5} m_1^{1/5} \dot{M}_{16}^{2/5} R_{10}^{-4/5} f^{8/5} A^{1/10} \text{ K}; \quad (\text{A.16})$$

$$\tau = 6.9 \times 10^4 \alpha^{-4/5} f^{-8/5} m_1^{-6/5} \dot{M}_{16}^{-2/5} R_{10}^{9/5} A^{7/10} B^{-2}; \quad (\text{A.17})$$

$$\eta = 4.3 \times 10^9 \alpha^{9/10} A^{-9/20} R_{10}^{3/5} m_1^{1/10} \dot{M}_{16}^{1/5} f^{4/5} \text{ cm}^2 \text{ s}^{-1}; \quad (\text{A.18})$$

$$v_R = 4.3 \times 10^{-1} \alpha^{9/10} A^{-9/20} R_{10}^{-2/5} m_1^{1/10} \dot{M}_{16}^{1/5} f^{4/5} \text{ cm s}^{-1}. \quad (\text{A.19})$$

Outer region: $P_{\text{gas}} \gg P_{\text{rad}}$ and $\kappa_{es} \ll \kappa_{ff}$:

$$\Sigma = 3.65 \alpha^{-4/5} A^{7/20} R_{10}^{-2/5} f^{14/5} B^{-9/10} \dot{M}_{16}^{7/10} m_1^{-1/10} \text{ g cm}^{-2}; \quad (\text{A.20})$$

$$H = 1.5 \times 10^8 \alpha^{-1/10} f^{3/5} \dot{M}_{16}^{3/20} R_{10}^{7/10} m_1^{1/20} A^{-17/40} B^{-1/20} \text{ cm}; \quad (\text{A.21})$$

$$\rho = 2.4 \times 10^{-8} \alpha^{-7/10} R_{10}^{-11/10} f^{11/5} \dot{M}_{16}^{11/20} m_1^{-3/20} A^{31/40} B^{-17/20} \text{ g cm}^{-3}; \quad (\text{A.22})$$

$$T_c = 2.5 \times 10^4 \alpha^{-1/5} R_{10}^{-3/5} \dot{M}_{16}^{3/10} f^{6/5} m_1^{1/10} A^{3/20} B^{-1/10} \text{ K}; \quad (\text{A.23})$$

$$\tau = 177 \alpha^{-4/5} R_{10}^{3/5} f^{4/5} \dot{M}_{16}^{1/5} m_1^{-3/5} A^{3/5} B^{-7/5}; \quad (\text{A.24})$$

$$\eta = 2.7 \times 10^{14} \alpha^{4/5} f^{6/5} \dot{M}_{16}^{3/10} R_{10}^{2/5} m_1^{1/10} A^{-7/20} B^{-1/10} \text{ cm}^2 \text{ s}^{-1}; \quad (\text{A.25})$$

$$v_R = 2.7 \times 10^4 \alpha^{4/5} f^{-14/5} \dot{M}_{16}^{3/10} R_{10}^{-3/5} m_1^{1/10} A^{-7/20} B^{9/10} \text{ cm s}^{-1}. \quad (\text{A.26})$$

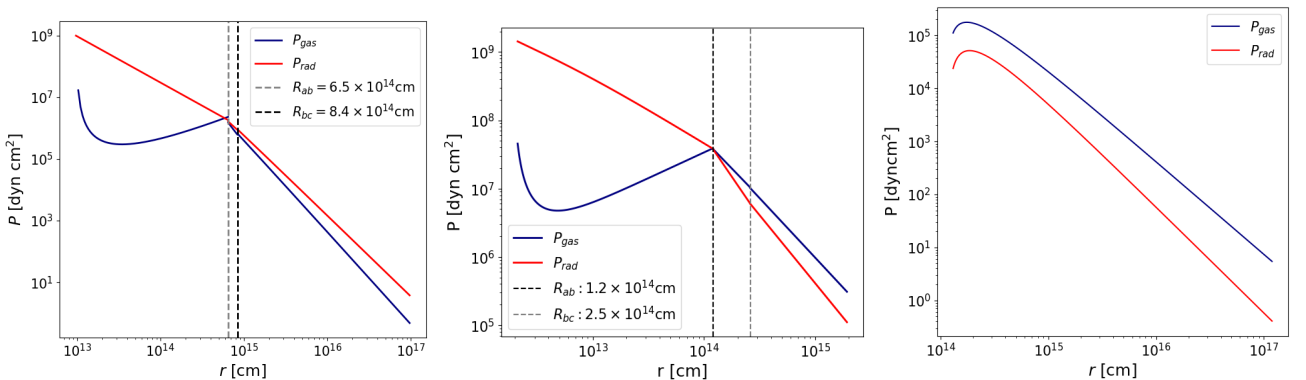


Fig. A.1: Variation of the radiation and gas pressures for a disc around a black hole (left), the RAR solution B2 (centre) and the RAR solution A2 (right). Dashed black and grey lines represent the limits of the different regions.

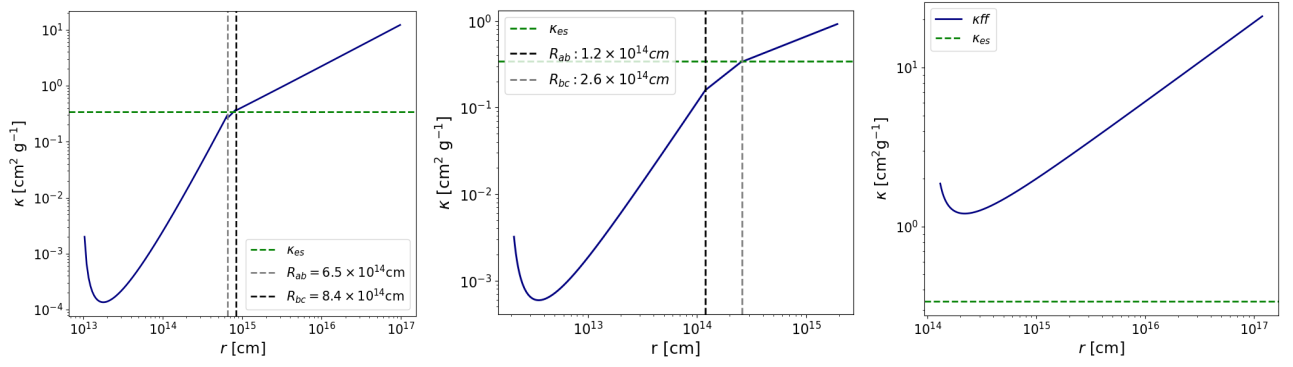


Fig. A.2: Variation of the absorption coefficients for a disc around a black hole (left), the RAR solution B2 (centre) and the RAR solution A2 (right). Dashed black and grey lines represent the limits of the different regions.

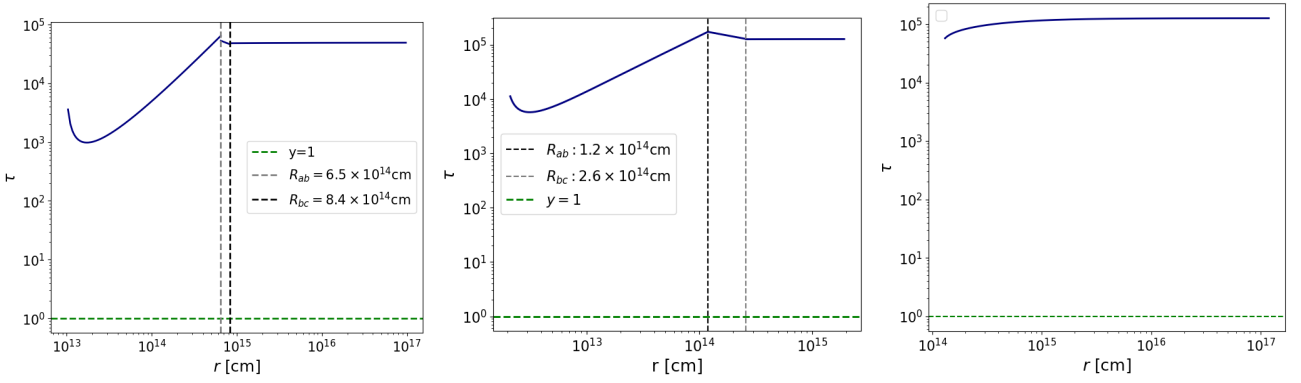


Fig. A.3: Variation of the opacity for a disc around a black hole (left), the RAR solution B2 (centre) and the RAR solution A2 (right). Dashed black and grey lines represent the limits of the different regions.

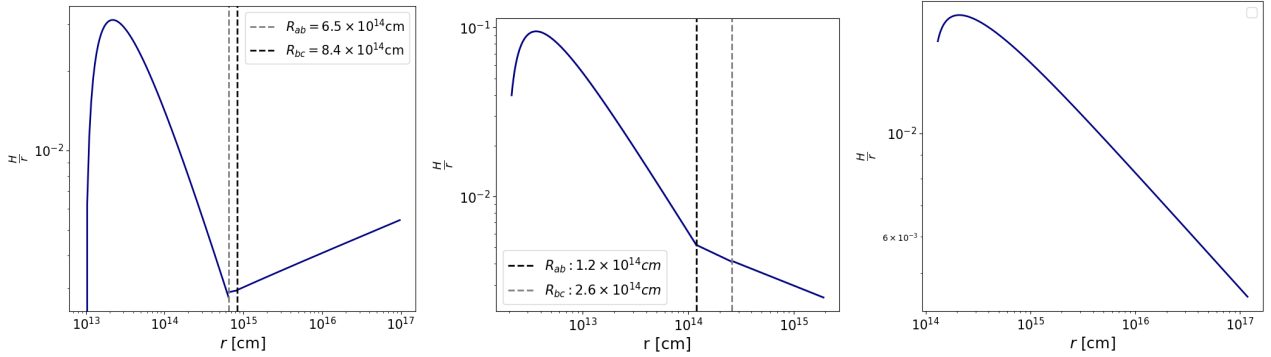


Fig. A.4: Thin disc approximation for a disc around a black hole (left), the RAR solution B2 (centre) and the RAR solution A2 (right). Dashed black and grey lines represent the limits of the different regions.